Multi-material topology optimization with multiple volume constraints: Combining the ZPR update with a ground-structure algorithm to select a single material per overlapping set

Article *in* International Journal for Numerical Methods in Engineering · November 2017

DOI: 10.1002/nme.5736

CITATIONS
13

READS
252

3 authors, including:

Xiaojia Shelly Zhang
University of Illinois, Urbana-Champaign
20 PUBLICATIONS **192** CITATIONS
SEE PROFILE

Adeildo Ramos Jr
Universidade Federal de Alagoas
5 PUBLICATIONS **13** CITATIONS
SEE PROFILE

Received: 27 May 2017 | Revised: 2 October 2017 | Accepted: 20 November 2017

DOI: 10.1002/nme.5736

RESEARCH ARTICLE

WILEY

Multimaterial topology optimization with multiple volume constraints: Combining the ZPR update with a ground-structure algorithm to select a single material per overlapping set

Xiaojia Shelly Zhang[1] | Glaucio H. Paulino[1] | Adeildo S. Ramos Jr.[2]

[1]School of Civil and Environmental Engineering, Georgia Institute of Technology, Atlanta, GA 30332, USA

[2]Laboratory of Scientific Computing and Visualization (LCCV), Technology Center, Federal University of Alagoas, Maceió, Brazil

Correspondence
Glaucio H. Paulino, School of Civil and Environmental Engineering, Georgia Institute of Technology, 790 Atlantic Drive, Atlanta, Georgia 30332, USA.
Email: paulino@gatech.edu

Funding information
US National Science Foundation (NSF), Grant/Award Number: 1559594; Raymond Allen Jones Chair at the Georgia Institute of Technology; Laboratory of Scientific Computing and Visualization (LCCV), Technology Center; Federal University of Alagoas (UFAL)

Summary

Multimaterial topology optimization often leads to members containing composite materials. However, in some instances, designers might be interested in using only one material for each member. Therefore, we propose an algorithm that selects a single preferred material from multiple materials per overlapping set. We develop the algorithm, based on the evaluation of both the strain energy and the cross-sectional area of each member, to control the material profile (ie, the number of materials) in each subdomain of the final design. This algorithm actively and iteratively selects materials to ensure that a single material is used for each member. In this work, we adopt a multimaterial formulation that handles an arbitrary number of volume constraints and candidate materials. To efficiently handle such volume constraints, we employ the ZPR (Zhang-Paulino-Ramos) design variable update scheme for multimaterial optimization, which is based upon the separability of the dual objective function of the convex subproblem with respect to Lagrange multipliers. We provide an alternative derivation of this update scheme based on the Karush-Kuhn-Tucker conditions. Through numerical examples, we demonstrate that the proposed material selection algorithm, which can be readily implemented in multimaterial optimization, along with the ZPR update scheme, is robust and effective for selecting a single preferred material among multiple materials.

KEYWORDS

ground structure method, material nonlinearity, material selection algorithm, multimaterial topology optimization, multiple volume constraints, ZPR update algorithm

1 | INTRODUCTION

Multimaterial topology optimization may lead to members containing more than one material. Thus, in this paper, we propose a material selection algorithm that ensures the selection of a single material for each member. This algorithm, based on the evaluation of both the strain energy and the cross-sectional area of each member, performs iteratively and

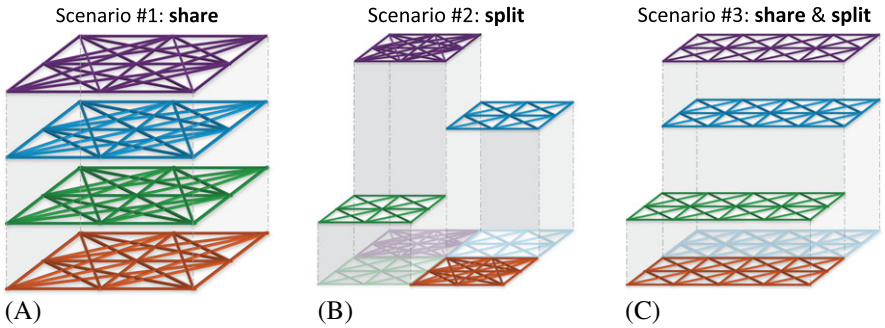

FIGURE 1 Ground structure combinations for material layers. (A) Scenario #1, in which 4 materials share the entire domain; (B) Scenario #2, in which 4 materials split the domain; (C) Scenario #3, in which 4 materials share and split the domain, enabling a general setting [Colour figure can be viewed at wileyonlinelibrary.com]

actively throughout the optimization process. In the context of truss layout optimization using the ground structure method (GSM), we consider 3 scenarios of the initial assignment of material layers. As shown in Figure 1, the multiple material layers can either share (Scenario #1) or split (Scenario #2) the design domain, or combine both (Scenario #3).

Through an illustrative example in Figure 2, we demonstrate the difference between optimization processes without controlling the number of materials in each subdomain (typical approach) and with controlling the selection of at most one material from each subdomain by using the proposed algorithm. The design domain and boundary conditions are provided in Figure 2A, whereas Figure 2B displays the material models in which *Material 1* has a larger Young's modulus than *Material 2* in both tension and compression regions. The initial ground structures (GS) of the 2 bilinear materials share the entire domain, and each material is assigned to an individual volume constraint. As demonstrated by Figure 2C, overlapping of 2 materials occurs in the optimized design when we allow the selection of more than one material. On the other hand, the final result of employing the material selection algorithm (Figure 2D), which ensures the selection of a single material, shows that each truss member in the optimized design contains at most one material.

Based on the aforementioned description, the remainder of this paper is organized as follows. Section 2 provides the motivation and a review of related work on multimaterial topology optimization. Section 3 describes the proposed multimaterial topology optimization formulation, followed by the sensitivity analysis and the incorporation of a discrete filter. Section 4 introduces an alternative derivation of the Zhang-Paulino-Ramos (ZPR) design variable update scheme, which is based on the Karush-Kuhn-Tucker (KKT) conditions. Section 5 proposes an algorithm that selects a single preferred material among multiple materials. Section 6 presents numerical examples in 2 and 3 dimensions, highlighting the properties of the proposed material selection algorithm, and Section 7 provides the concluding remarks.

2 | MOTIVATION AND RELATED WORK

Topology optimization with multiple materials is a powerful design tool because it not only finds the optimal topology but also selects the proper type and amount of materials. One common feature of practical engineering designs is that they typically consist of multiple material types such as high-rise buildings and composite materials in the macroscale and microscale, respectively. The literature on multimaterial topology optimization mainly deals with the continuum setting such as the density-based approach. Various generalizations and extensions of the solid isotropic material with penalization[1] and other material interpolation schemes in the single-material topology optimization are made to accommodate multiple materials (see for example other studies[2-6]). In addition to density-based formulations, phase-field[7-9] and level set[10-13] approaches are also used for multimaterial topology optimization formulations.

In addition to the continuum setting, some studies perform multimaterial topology optimization using discrete elements, eg, truss and lattice networks. Among these studies, most focus on integrating truss elements into continuum topology optimization for the purpose of designing reinforced concrete structures and strut-and-tie models (see for example these studies[14-18]). However, few multimaterial topology optimization studies focus on truss networks using the GSM.

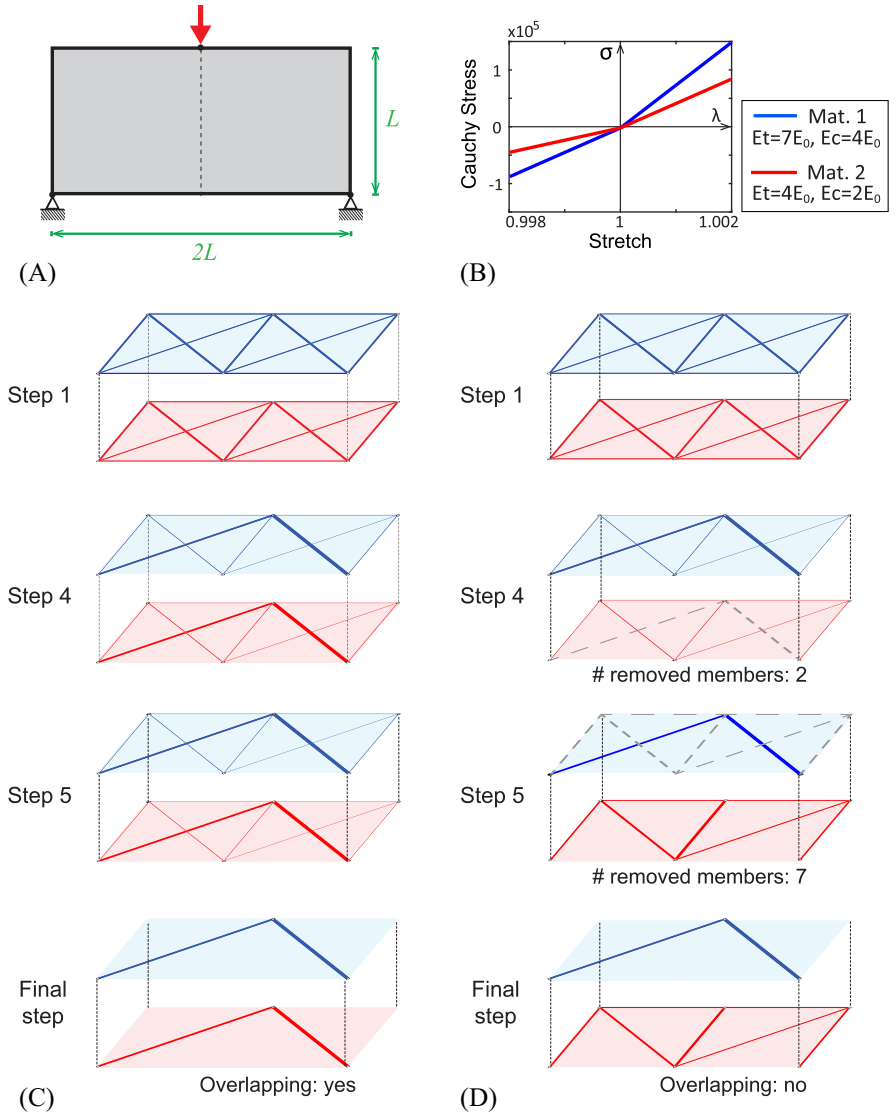

FIGURE 2 Demonstration of the algorithm that selects a single material among multiple materials at each subdomain. (A) Design domain; (B) 2 bilinear material models, ie, *Material 1* has a larger Young's modulus than *Material 2* in both tension and compression regions; (C) multimaterial topology optimization that allows the selection of more than one material from each subdomain; (D) multimaterial topology optimization with the algorithm that selects at most one material from each subdomain. Dotted lines represent removed members

Another limitation in multimaterial topology optimization literature is that it mostly assumes material linearity, yet real materials generally display nonlinear constitutive relations. In addition, most studies on multimaterial topology optimization use a limited setting for volume constraints. These studies either assign a total volume constraint for all candidate materials (for example, see studies[4,6,14-17]), which may cause issues if linear materials are used, or assign an individual volume constraint to each material (for example, see studies[2,3,7-10,12]), which may impose higher computational demand on formulation and update scheme implementations. A general setting, ie, the combination of both types of constraints for various design purposes, and a tailored update scheme that handles arbitrary volume constraints are needed in multimaterial optimization.

To address the aforementioned limitations, we adopt our multimaterial topology optimization framework[19] utilizing the ZPR update scheme, which can handle an arbitrary number of candidate materials with flexible material properties and a general setting of volume constraints. The ZPR design variable update scheme separates the updates of the design variables associated with each volume constraint and performs updates independently in series or in parallel. The update scheme is derived based on the separable feature of the dual objective function of the convex subproblem with respect to

the Lagrange multipliers. The update of design variables thus depends only on the Lagrange multiplier of its associated volume constraint.*Thus, the ZPR update scheme is capable of handling an arbitrary number of volume constraints while preserving efficiency. In addition to volume constraints, the ZPR update scheme can be used to handle other types of linear constraints.*

The adopted multimaterial formulation may lead to members containing more than 1 material (ie, members with composite materials). In general, this phenomenon occurs under 3 conditions, which need to be satisfied simultaneously. *First*, 2 or more materials are assigned to share a domain in the initial material assignment (eg, the initial GS in Figure 1A,C). *Second,* among the materials that share a domain, one material is stronger at least within a certain range of stretch values (eg, in Figure 2B, *Material 1* is stronger than *Material 2* in the entire range of stretch values). *Third,* these materials are associated with individual volume constraints.

In the literature, several attempts have been made in continuum multimaterial topology optimization to overcome the issues of selecting more than one material. One common strategy is to consider the *product interpolation* in the discrete material optimization technique,[5] which is based on a penalization scheme. However, this approach does not completely eliminate selecting of multiple materials at subdomains, especially at material interfaces. In order to enforce the selection of at most or exactly one material at each design subdomain, material selection constraints are introduced by employing discrete variables, which converts the optimization to a mixed integer problem (see for example the work of Hvejsel and Lund[4]). In the context of truss topology optimization with multiple materials, the above-reviewed approaches cannot be directly nor efficiently adopted, and currently, no work allows for control of the material profile (ie, number of materials) in each truss member of the final design.

The goal of this paper is to propose an effective algorithm that enforces a single material selection in each subdomain in the multimaterial topology optimization of trusses. We highlight that the proposed algorithm is active and iterative in nature and performed throughout the optimization process. This is conceptually different from the following 2 postprocessing approaches. Postprocessing of the final designs with composite materials, ie, removing truss members with less contribution at the end of the optimization step, causes a decrease in volume and an increase in displacement and, most importantly, may remove all the truss members with less favorable materials leading to designs only containing the most favorable material. Additionally, treating all composite members at the same time may, again, lead to designs only containing the most favorable material.

3 | MULTIMATERIAL TOPOLOGY OPTIMIZATION

This section introduces the adopted multimaterial topology optimization formulation and its sensitivity analysis, followed by the incorporation of a discrete filter. Within the context of the GSM and assuming a total of m candidate materials, the framework consists of m layers of initial GS. We assume that the ith GS layer with material i (where $i = 1, \dots, m$ is the material index) contains M_i truss members and denotes $\boldsymbol{x}_i$ as the associated vector of design variables. The eth design variable component, ie, $x_i^{(e)}$, is the cross-sectional area of the eth truss member of material i. Additionally, the formulation contains nc independent volume constraints, where $1 \leq nc \leq m$. For the jth volume constraint, we denote $\mathcal{G}^j$ as the set of material indices associated with that volume constraint.

The formulation for such multimaterial truss topology optimization is given as follows:

$$\begin{aligned}
\min_{\boldsymbol{x}_1,\dots,\boldsymbol{x}_m} \; & J(\boldsymbol{x}_1, \dots, \boldsymbol{x}_m) = \min_{\boldsymbol{x}_1,\dots,\boldsymbol{x}_m} -\Pi(\boldsymbol{x}_1, \dots, \boldsymbol{x}_m, \boldsymbol{u}(\boldsymbol{x}_1, \dots, \boldsymbol{x}_m)) \\
\text{s.t. } & g^j(\boldsymbol{x}_1, \dots, \boldsymbol{x}_m) = \sum_{i \in \mathcal{G}^j} \boldsymbol{L}_i^{\mathrm{T}} \boldsymbol{x}_i - V_{\max}^j \leq 0, \; j = 1, \dots, nc, \\
& x_{\min} \leq x_i^{(e)} \leq x_{\max}, \; i = 1, \dots, m, \text{ and } e = 1, \dots, M_i, \\
\text{with } & \boldsymbol{u}(\boldsymbol{x}_1, \dots, \boldsymbol{x}_m) = \arg\min_{\boldsymbol{u}} \Pi(\boldsymbol{x}_1, \dots, \boldsymbol{x}_m, \boldsymbol{u}),
\end{aligned} \tag{1}$$

where J is the objective function; $\boldsymbol{u}(\boldsymbol{x}_1, \dots, \boldsymbol{x}_m)$ is the equilibrating displacement field (state variable); Π is the total potential energy; $V_{\max}^j$ is the prescribed upper bound on the total volume associated with the jth volume constraint, g^j; $x_{\min}$, and $x_{\max}$ are the prescribed lower and upper bounds of the design variables; and $\boldsymbol{L}_i$ is the length vector of the ith material. As a demonstration of the notation in multimaterial optimization formulation (1), Figure 3 and Table 1 summarize the parameters for a case with 3 materials ($m = 3, M_1 = 5, M_2 = 5$, and $M_3 = 9$) and 2 volume constraints ($nc = 2$, $\mathcal{G}^1 = \{1\}, \mathcal{G}^2 = \{2, 3\}$).

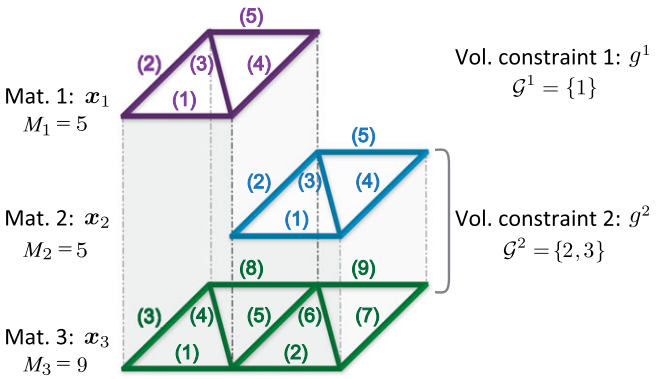

FIGURE 3 Parameters in the multimaterial optimization formulation. Three materials share and split the design domain ($m = 3$, $M_1 = 5, M_2 = 5$, and $M_3 = 9$) with 2 volume constraints (*Material 1* has an individual volume constraint, whereas *Material 2* and *Material 3* share 1 volume constraint, $nc = 2, \mathcal{G}^1 = \{1\}, \mathcal{G}^2 = \{2,3\}$) [Colour figure can be viewed at wileyonlinelibrary.com]

TABLE 1 Parameters in multimaterial optimization formulation (Figure 3)

Materials, $m = 3$	M_i	$x_i = \left\{x_i^{(e)}\right\}^T, \quad i = 1, \dots, m, \quad e = 1, \dots, M_i$
1	$M_1 = 5$	$x_1 = \left\{x_1^{(1)}, x_1^{(2)}, x_1^{(3)}, x_1^{(4)}, x_1^{(5)}\right\}^T$
2	$M_2 = 5$	$x_2 = \left\{x_2^{(1)}, x_2^{(2)}, x_2^{(3)}, x_2^{(4)}, x_2^{(5)}\right\}^T$
3	$M_3 = 9$	$x_3 = \left\{x_3^{(1)}, x_3^{(2)}, x_3^{(3)}, x_3^{(4)}, x_3^{(5)}, x_3^{(6)}, x_3^{(7)}, x_3^{(8)}, x_3^{(9)}\right\}^T$
Volume constraints, $nc = 2$	$\mathcal{G}^j$	$g^j = \sum_{i \in \mathcal{G}^j} L_i^T x_i - V_{\max}^j \le 0, \quad j = 1, \dots, nc$
1	$\mathcal{G}^1 = \{1\}$	$g^1 = L_1^T x_1 - V_{\max}^1 \le 0$
2	$\mathcal{G}^2 = \{2,3\}$	$g^2 = L_2^T x_2 + L_3^T x_3 - V_{\max}^2 \le 0$

In the above topology optimization formulation, we aim to maximize the total potential energy of the multimaterial truss system in its equilibrium state. The total potential energy Π of the truss system is defined as the difference of the total internal strain energy and the external work done by the applied force $\boldsymbol{f}$. More explicitly, the total potential energy Π is defined as

$$\Pi(\boldsymbol{x}_1, \dots, \boldsymbol{x}_m, \boldsymbol{u}) = \sum_{i=1}^{m} \sum_{e=1}^{M_i} x_i^{(e)} L_i^{(e)} \Psi_i^{(e)}(\boldsymbol{u}) - \boldsymbol{f}^T \boldsymbol{u}, \tag{2}$$

where $\Psi_i^{(e)}(\boldsymbol{u})$ is the strain energy density function of truss member e in material i, $L_i^{(e)}$ is the length of that truss member, and $\boldsymbol{f}$ is the external force vector. In this work, we assume small deformation and nonlinear constitutive relations provided that the strain energy density function, ie, $\Psi_i^{(e)}(\boldsymbol{u})$, is convex and differentiable for any given $\boldsymbol{u}$. We account for the nonlinear constitutive relationship through the Ogden-based model[20] and the bilinear model. The strain energy density function for the Ogden-based model is given by

$$\Psi_{OG}(\lambda) = \sum_{j=1}^{M} \frac{\gamma_j}{\beta_j} \left(\lambda^{\beta_j} - 1\right), \tag{3}$$

where λ denote the axial stretch and M, γ_j, and β_j are material parameters. By varying the material parameters, the Ogden-based model allows control of the constitutive relationships and has the capability to reproduce a variety of hyperelastic materials. The strain energy density function for the bilinear model is defined as

$$\Psi_{Bi}(\lambda) = \begin{cases} \frac{1}{2} E_t (\lambda - 1)^2, & \text{if } \lambda > 1, \\ \frac{1}{2} E_c (\lambda - 1)^2, & \text{otherwise}, \end{cases} \tag{4}$$

where E_t and E_c are Young's moduli for tension and compression, respectively. For more details of these material models, readers are referred to the studies of Ramos et al[21] and Zhang et al.[22]

Next, we provide the sensitivity information of the objective function and volume constraints. Because $\boldsymbol{u}(\boldsymbol{x}_1, \ldots, \boldsymbol{x}_m)$ is the equilibrating displacement, the sensitivity of the objective function with respect to each design variable is obtained as[19]

$$\frac{\partial J}{\partial x_i^{(e)}}(\boldsymbol{x}_1, \ldots, \boldsymbol{x}_m) = -L_i^{(e)} \Psi_i^{(e)}(\boldsymbol{u}(\boldsymbol{x}_1, \ldots, \boldsymbol{x}_m)), \tag{5}$$

which does not involve any adjoint vector. Additionally, the sensitivity of the jth volume constraint is expressed as

$$\frac{\partial g^j(\boldsymbol{x}_1, \ldots, \boldsymbol{x}_m)}{\partial x_i^{(e)}} = \begin{cases} L_i^{(e)}, & \text{if} \quad i \in \mathcal{G}^j, \\ 0, & \text{otherwise.} \end{cases} \tag{6}$$

The multimaterial topology optimization formulation (1) has several features. It is capable of handling an arbitrary number of materials with flexible initial material assignment (ie, the materials can either share or split the design domain or combine both) and independent constitutive relations (eg, each candidate material can be either linear, bilinear, or nonlinear). The assignment of volume constraints is general; we can assign a total/global volume constraint to all the materials, an individual volume constraint to each material, or a combination of both.

The discrete filtering technique in the GSM is proposed in the work of Ramos Jr and Paulino[23] and is extended in the work of Zhang et al[22] to problems considering nonlinear materials. The discrete filtering allows users to control the resolution of the design and ensure the global equilibrium of the final topology. For optimization with nonlinear structural analysis, the discrete filtering is further shown to significantly improve computational efficiency.[22] Therefore, in this work, the discrete filtering technique is incorporated in the multimaterial optimization formulation.

We define a user-defined parameter α_f that represents the minimal allowed resolution in the final topology, the filter operation is defined as follows:

$$\text{Filter}\left(\boldsymbol{x}, \alpha_f, e\right) = \begin{cases} 0, & \text{if} \quad \frac{x^{(e)}}{\max(\boldsymbol{x})} < \alpha_f < 1, \\ x^{(e)}, & \text{otherwise.} \end{cases} \tag{7}$$

The above filter operation is used with a reduced-order modeling scheme, which removes the information associated with the set of truss members displaying normalized areas below α_f in both the nonlinear structural system analysis (the state problem) and the optimization analysis. In this manuscript, we consider small filter values, eg, 10^{-3} or 10^{-4}, which has been shown in the work of Zhang et al[22] to yield almost identical results to the ones obtained without the discrete filter.

Incorporating the discrete filtering technique, the multimaterial topology optimization formulation in (1) is modified as

$$\begin{aligned} \min_{\boldsymbol{x}_1, \ldots, \boldsymbol{x}_m} \; & J(\boldsymbol{x}_1, \ldots, \boldsymbol{x}_m) = \min_{\boldsymbol{x}_1, \ldots, \boldsymbol{x}_m} -\Pi\left(\overline{\boldsymbol{x}}_1(\boldsymbol{x}_1), \ldots, \overline{\boldsymbol{x}}_m(\boldsymbol{x}_m), \boldsymbol{u}(\boldsymbol{x}_1, \ldots, \boldsymbol{x}_m)\right) \\ \text{s.t.} \; & g^j(\boldsymbol{x}_1, \ldots, \boldsymbol{x}_m) = \sum_{i \in \mathcal{G}^j} L_i^{\mathrm{T}} \overline{\boldsymbol{x}}_i(\boldsymbol{x}_i) - V_{\max}^j \le 0, \; j = 1, \ldots, nc, \\ & 0 \le x_i^{(e)} \le x_{\max}, \; i = 1, \ldots, m, \text{and} \, e = 1, \ldots, M_i, \\ \text{with} \; & \boldsymbol{u}(\boldsymbol{x}_1, \ldots, \boldsymbol{x}_m) = \arg\min_{\boldsymbol{u}} \left\{ \Pi\left(\overline{\boldsymbol{x}}_1(\boldsymbol{x}_1), \ldots, \overline{\boldsymbol{x}}_m(\boldsymbol{x}_m), \boldsymbol{u}\right) + \frac{\Gamma}{2} \boldsymbol{u}^{\mathrm{T}} \boldsymbol{u} \right\}, \\ & \overline{x}_i^{(e)} = \text{Filter}\left(\boldsymbol{x}_i, \alpha_f, e\right), \; i = 1, \ldots, m, \text{and} \, e = 1, \ldots, M_i, \end{aligned} \tag{8}$$

where the filter operation is applied to the design variables associated with each material set and $\overline{\boldsymbol{x}}_i$ denotes the filtered design variable associated with the ith material. We note that the modified formulation (8) relaxes the lower bound of design variables to $x_{\min} = 0$ to account for the removal of members. Thus, a Tikhonov regularization term $(\Gamma/2)\boldsymbol{u}^{\mathrm{T}}\boldsymbol{u}$ is needed in the total potential energy to prevent singular tangent stiffness matrices[23-26] in the structural equations.

4 | ALT-ZPR: ALTERNATIVE DERIVATION OF THE ZPR UPDATE SCHEME

The Zhang-Paulino-Ramos or ZPR (zipper, phonetically) design variable update scheme[19] is adopted here for multimaterial topology optimization. This design variable update scheme is capable of updating an arbitrary number of volume constraints while preserving efficiency and robustness. In particular, the ZPR update scheme separately and independently updates the design variables associated with each volume constraint.

The derivation of the ZPR update scheme that utilizes primal-dual relationship is presented in the work of Zhang et al.[19] Here, we show an alternative derivation of this update scheme using the KKT conditions. At each optimization step k, we introduce a convex approximation of the objective function over the intervening variable $\boldsymbol{y}_i(\boldsymbol{x}_i)$ such that $y_i^{(e)}(x_i^{(e)}) = (x_i^{(e)})^{-\alpha}$, $i = 1, \dots, m$ and $e = 1, \dots, M_i$, as follows:

$$\begin{aligned} J(\boldsymbol{x}_1, \dots, \boldsymbol{x}_m) \approx J^k(\boldsymbol{x}_1, \dots, \boldsymbol{x}_m) &= J\left(\boldsymbol{x}_1^k, \dots, \boldsymbol{x}_m^k\right) + \sum_{i=1}^{m}\left[\frac{\partial J}{\partial \boldsymbol{y}_i}(\boldsymbol{x}_1^k, \dots, \boldsymbol{x}_m^k)\right]^T \left[\boldsymbol{y}_i(\boldsymbol{x}_i) - \boldsymbol{y}_i(\boldsymbol{x}_i^k)\right] \\ &= J\left(\boldsymbol{x}_1^k, \dots, \boldsymbol{x}_m^k\right) + \sum_{i=1}^{m}\left[\boldsymbol{b}_i(\boldsymbol{x}_1^k, \dots, \boldsymbol{x}_m^k)\right]^T \left[\boldsymbol{y}_i(\boldsymbol{x}_i) - \boldsymbol{y}_i(\boldsymbol{x}_i^k)\right], \end{aligned} \tag{9}$$

where α is a strictly positive arbitrary number, $\boldsymbol{x}_i^k$ and $\boldsymbol{y}_i(\boldsymbol{x}_i^k)$ are the design and intervening variables at the kth optimization step for material i, and $b_i(\boldsymbol{x}_1^k, \dots, \boldsymbol{x}_m^k)$ is a constant vector, whose component is given as the following function of the corresponding eth component of the sensitivity vector:

$$b_i^{(e)}\left(\boldsymbol{x}_1^k, \dots, \boldsymbol{x}_m^k\right) = \frac{\partial J}{\partial y_i^{(e)}}\left(\boldsymbol{x}_1^k, \dots, \boldsymbol{x}_m^k\right) = -\frac{\left(x_i^{(e),k}\right)^{1+\alpha}}{\alpha}\frac{\partial J}{\partial x_i^{(e)}}\left(\boldsymbol{x}_1^k, \dots, \boldsymbol{x}_m^k\right). \tag{10}$$

Using the approximated objective function J^k, we obtain a subproblem at step k formulated as follows:

$$\begin{aligned} \min_{\boldsymbol{x}_1, \dots, \boldsymbol{x}_m} J^k(\boldsymbol{x}_1, \dots, \boldsymbol{x}_m) &= \min_{\boldsymbol{x}_1, \dots, \boldsymbol{x}_m} J\left(\boldsymbol{x}_1^k, \dots, \boldsymbol{x}_m^k\right) + \sum_{i=1}^{m}\left[\frac{\partial J}{\partial \boldsymbol{y}_i}\left(\boldsymbol{x}_1^k, \dots, \boldsymbol{x}_m^k\right)\right]^T \left[\boldsymbol{y}_i(\boldsymbol{x}_i) - \boldsymbol{y}_i\left(\boldsymbol{x}_i^k\right)\right] \\ \text{s.t.} \sum_{i \in \mathcal{G}^j} L_i^{\mathrm{T}} \boldsymbol{x}_i - V_{\max}^j &\le 0,\ j = 1, \dots, nc, \\ x_{i,\mathrm{L}}^{(e),k} \le x_i^{(e)} &\le x_{i,\mathrm{U}}^{(e),k},\ i = 1, \dots, m, \text{and } e = 1, \dots, M_i, \\ \text{with } y_i^{(e)}\left(x_i^{(e)}\right) &= (x_i^{(e)})^{-\alpha},\ i = 1, \dots, m, \text{and } e = 1, \dots, M_i, \end{aligned} \tag{11}$$

where $\mathcal{G}^j$ is the set of material indices associated with jth volume constraint, and $x_{i,\mathrm{L}}^{(e),k} = \max(x_{\min}, x_i^{(e),k} - move)$ and $x_{i,\mathrm{U}}^{(e),k} = \min(x_{\max}, x_i^{(e),k} + move)$ are the lower and upper bounds of the design variables that are determined through the prescribed allowable move limit, ie, *move*.

By introducing a set of Lagrange multipliers ϕ_V^j, $j = 1, \dots, nc$, the Lagrangian of the subproblem in Equation (11) takes the following form:

$$\mathcal{L}\left(\boldsymbol{x}_1, \dots, \boldsymbol{x}_m, \phi_V^1, \dots, \phi_V^{nc}\right) = \sum_{i=1}^{m}\left[\boldsymbol{b}_i\left(\boldsymbol{x}_1^k, \dots, \boldsymbol{x}_m^k\right)\right]^T \boldsymbol{y}_i(\boldsymbol{x}_i) + \sum_{j=1}^{nc}\phi_V^j\left(\sum_{i \in \mathcal{G}^j} L_i^{\mathrm{T}}\boldsymbol{x}_i - V_{\max}^j\right). \tag{12}$$

Notice that the above Lagrangian is a separable function for each volume constraint, ie,

$$\begin{aligned} \mathcal{L}\left(\boldsymbol{x}_1, \dots, \boldsymbol{x}_m, \phi_V^1, \dots, \phi_V^{nc}\right) &= \sum_{j=1}^{nc}\mathcal{L}^j\left(\boldsymbol{x}_i, \dots, \boldsymbol{x}_m, \phi_V^j\right) \\ &= \sum_{j=1}^{nc}\left\{\sum_{i \in \mathcal{G}^j}\left[\left[\boldsymbol{b}_i\left(\boldsymbol{x}_1^k, \dots, \boldsymbol{x}_m^k\right)\right]^T \boldsymbol{y}_i(\boldsymbol{x}_i) + \phi_V^j \boldsymbol{L}_i^{\mathrm{T}}\boldsymbol{x}_i\right] - \phi_V^j V_{\max}^j\right\}. \end{aligned} \tag{13}$$

The KKT conditions of the subproblem (11) require that

$$\frac{\partial \mathcal{L}}{\partial x_i^{(e)}} = \frac{\partial \mathcal{L}^j}{\partial x_i^{(e)}} = -\alpha b_i^{(e)}\left(\boldsymbol{x}_1^k, \dots, \boldsymbol{x}_m^k\right)\left(x_i^{(e)}\right)^{(-\alpha-1)} + \phi_V^j L_i^{(e)} = 0, \quad \forall i \in \mathcal{G}^j, \tag{14}$$

and

$$\frac{\partial \mathcal{L}}{\partial \phi_V^j} = \sum_{i \in \mathcal{G}^j} L_i^{\mathrm{T}}\boldsymbol{x}_i - V_{\max}^j = 0, \quad j = 1, \dots, nc. \tag{15}$$

We denote $x_i^{(e)*}$ as the solution of the aforementioned KKT conditions. From (14), we can write the solution $x_i^{(e)*}$ as

$$x_i^{(e)*} = Q_i^{(e),k}\left(\phi_V^j\right) = \left[\frac{\alpha b_i^{(e)}\left(\boldsymbol{x}_1^k, \ldots, \boldsymbol{x}_m^k\right)}{\phi_V^j L_i^{(e)}}\right]^{\frac{1}{1+\alpha}}, \quad \forall i \in \mathcal{G}^j. \tag{16}$$

By further incorporating the lower and upper bounds, ie, $\boldsymbol{x}_{i,\mathrm{L}}^k$, and $\boldsymbol{x}_{i,\mathrm{U}}^k$, of the design variables, the expression for $x_i^{(e)*}$ is modified as

$$x_i^{(e)*} = Q_i^{(e),k}\left(\phi_V^j\right) = \begin{cases} x_{i,\mathrm{L}}^{(e),k}, & \text{if } \left[\frac{\alpha b_i^{(e)}\left(\boldsymbol{x}_1^k, \ldots \boldsymbol{x}_m^k\right)}{\phi_V^j L_i^{(e)}}\right]^{\frac{1}{1+\alpha}} < x_{i,\mathrm{L}}^{(e),k} \\ \left[\frac{\alpha b_i^{(e)}\left(\boldsymbol{x}_1^k, \ldots \boldsymbol{x}_m^k\right)}{\phi_V^j L_i^{(e)}}\right]^{\frac{1}{1+\alpha}}, & \text{if } x_{i,\mathrm{L}}^{(e),k} \le \left[\frac{\alpha b_i^{(e)}\left(\boldsymbol{x}_1^k, \ldots \boldsymbol{x}_m^k\right)}{\phi_V^j L_i^{(e)}}\right]^{\frac{1}{1+\alpha}} \le x_{i,\mathrm{U}}^{(e),k} \\ x_{i,\mathrm{U}}^{(e),k}, & \text{if } \left[\frac{\alpha b_i^{(e)}\left(\boldsymbol{x}_1^k, \ldots \boldsymbol{x}_m^k\right)}{\phi_V^j L_i^{(e)}}\right]^{\frac{1}{1+\alpha}} > x_{i,\mathrm{U}}^{(e),k} \end{cases}, \quad \forall i \in \mathcal{G}^j. \tag{17}$$

By plugging (17) back into Equation (15), we obtain

$$\frac{\partial \mathcal{L}}{\partial \phi_V^j} = \sum_{i \in \mathcal{G}^j} \sum_{e=1}^{M_i} L_i^{(e)} x_i^{(e)*}\left(\phi_V^j\right) - V_{\max}^j = 0, \quad j = 1, \ldots, nc. \tag{18}$$

Notice that the jth equation of the aforementioned system is an algebraic equation as a function ϕ_V^j; therefore, each optimal Lagrange multiplier ϕ_V^{j*} can be solved independently by its corresponding equation. We then have a decoupled system with respect to the volume constraints.

Finally, the update of the eth component of design variables $\boldsymbol{x}_i^{k+1}$ is taken as the optimal solution in subproblem (11) as follows:

$$x_i^{(e),k+1} = Q_i^{(e),k}\left(\phi_V^{j*}\right), \quad \forall i \in \mathcal{G}^j. \tag{19}$$

When applied to the multimaterial optimization problem in Section 3, the ZPR design variable update scheme in Equation (19) takes the following specific form:

$$x_i^{(e),k+1} = \begin{cases} x_{i,\mathrm{L}}^{(e),k} & \text{if } \left[\frac{\Psi_i^{(e)}\left(u\left(\boldsymbol{x}_1^k, \ldots \boldsymbol{x}_m^k\right)\right)}{\phi_V^{j*}}\right]^{\eta} x_i^{(e),k} < x_{i,\mathrm{L}}^{(e),k} \\ \left[\frac{\Psi_i^{(e)}\left(u\left(\boldsymbol{x}_1^k, \ldots \boldsymbol{x}_m^k\right)\right)}{\phi_V^{j*}}\right]^{\eta} x_i^{(e),k} & \text{if } x_{i,\mathrm{L}}^{(e),k} \le \left[\frac{\Psi_i^{(e)}\left(u\left(\boldsymbol{x}_1^k, \ldots \boldsymbol{x}_m^k\right)\right)}{\phi_V^{j*}}\right]^{\eta} x_i^{(e),k} \le x_{i,\mathrm{U}}^{(e),k} \\ x_{i,\mathrm{U}}^{(e),k} & \text{if } \left[\frac{\Psi_i^{(e)}\left(u\left(\boldsymbol{x}_1^k, \ldots \boldsymbol{x}_m^k\right)\right)}{\phi_V^{j*}}\right]^{\eta} x_i^{(e),k} > x_{i,\mathrm{U}}^{(e),k} \end{cases}, \quad \forall i \in \mathcal{G}^j, \tag{20}$$

where $\eta = 1/(1+\alpha)$, which is commonly known as the damping factor. This factor can be either constant[27] or adaptive.[28]

We note that, from Equations (19) and (20), the updates of design variables are also decoupled in the sense that the update corresponding to the jth volume constraint only depends on its associated optimal Lagrange multiplier, ie, ϕ_V^{j*}. This feature, along with the decoupled solution of ϕ_V^{j*} in (18), allows the associated design variables of each volume constraint to be updated independently, highlighting one of the main advantages of the ZPR design variable update scheme.

5 | ALGORITHM TO SELECT A SINGLE PREFERRED MATERIAL PER OVERLAPPING SET

As discussed in Section 2, under the conditions that (i) multiple materials share the design domain, (ii) one of the materials (at least partially) dominates the others, and (iii) each of those materials is assigned with an individual volume constraint, optimization formulations (1) and (8) may lead to final topologies with overlapping sets/connectivities. This is shown in the optimized structure in Figure 2C. An overlapping set/connectivity is defined as the truss members with different

material properties and with nonzero cross-sectional areas that share the same end nodes. The presence of overlapping connectivities may lead to difficulties in defining a unique material property of each truss member in the final topology. In this section, we propose a simple and effective material selection algorithm to ensure that each connectivity (truss member) of the final topology contains at most one material. The basic concept and procedure of the proposed algorithm are illustrated by the example in Figure 2.

Assume that, at a given optimization step, we have identified all sets of overlapping members. Each of these sets contains all the nonzero area members that share the same end nodes. The basic idea of the material selection algorithm is to select the best member within each set according to a predefined criterion and remove other members. The removal is performed by assigning member cross-sectional areas to zero and applying Tikhonov regularization in the structural analysis to regularize the tangent stiffness matrices (regardless of whether the discrete filter is used). Notice that, when a member is removed, the total volume of the associated material decreases, and thus, the optimizer assigns the removed materials to other locations in the following optimization steps. By doing this, the optimization effectively redistributes the overlapped materials to other locations. If all the overlapped members at one material layer are removed at the same time, there might be no available members from that material layer to redistribute to the design (because each candidate material can only be redistributed within its associated material layer). To prevent this, a threshold (parameter), ie, $\alpha_{\text{select}} \in [0, 1]$, is defined such that this removing-and-redistributing procedure is performed gradually. In the material selection algorithm, the threshold is applied as follows. The normalized area of each member (the ratio of the cross-sectional area to the maximum cross-sectional area in its associated material layer) is first computed, and the removal is then performed to the overlapping sets whose ratios are larger than (or equal to) the aforementioned prescribed threshold α_{select}.

We adopt uniform area distribution as the initial guess for design variables, ie, the initial ratio of the member area to the maximum area of the corresponding material layer is one. As a result, if the selection algorithm is applied at the initial optimization step, all overlapping connectivities will be immediately removed according to the previously defined threshold. Additionally, no redistribution of the removed material can be done in the subsequent optimization steps. To avoid this, we allow the optimizer to freely develop topologies with nonuniform member areas and initiate the material selection algorithm after N_{select} optimization steps.

In addition to the parameters α_{select} and N_{select}, a criterion needs to be defined to determine the best member among the multiple materials in each overlapping set. In this work, we define the criterion to be the strain energy of the member per unit length, ie, $x\Psi$ (because the overlapping connectivities have the same lengths, the member length L is excluded in the criterion). For a set of overlapping members, we select the member with the largest strain energy (per unit length). The choice of this criterion is consistent with the objective function in (2) because members with larger strain energy (per unit length) contribute to larger total potential energy of the entire structure. Thus, members with larger strain energy are preferred because they are more efficient. More specifically, the proposed material selection algorithm follows the steps listed as follows.

1. Detect all sets of overlapping members (connectivities with more than one material selection).
2. Within each overlapping set, detect the member with the largest strain energy per unit length.
3. For this detected member in the current set, if its normalized cross-sectional area (with respect to the maximum cross-sectional area in its associated material layer) exceeds or equals to the prescribed threshold α_{select}, go to Step 4; otherwise, go to Step 5.
4. Select the member that has the largest strain energy per unit length and keep its cross-sectional area. Remove other members in the current set by assigning their cross-sectional areas to be zero.
5. Proceed to the next overlapping set.

To formalize the proposed algorithm, we introduce the following notation. Assuming that there are in total of p overlapping sets, we denote $\widetilde{\boldsymbol{x}}_j$ as the vector containing all the design variables in the jth set, where $\tilde{x}_j^{(i)}$ is the ith component of $\widetilde{\boldsymbol{x}}_j$. Accordingly, the vector of corresponding material indices of the jth set is defined as $\widetilde{\boldsymbol{m}}_j$ with its ith component denoted as $\tilde{m}_j^{(i)}$. The associated energy density function is denoted as $\Psi_{\tilde{m}_j^{(i)}}$. As an illustration, Figure 4 shows the overlapping of 3 materials at a connectivity (subdomain) and the corresponding notation. A design consisting of overlapping materials is shown in Figure 4A. The first overlapping set/connectivity consists of the fourth member of *Material 1*, the 2nd member of *Material 2*, and the fifth member of *Material 3*, as shown in Figure 4B; therefore, we write $\widetilde{\boldsymbol{x}}_1 = \{\widetilde{x}_1^{(1)}, \widetilde{x}_1^{(2)}, \widetilde{x}_1^{(3)}\}^T = \{x_1^{(4)}, x_2^{(2)}, x_3^{(5)}\}^T$ and $\widetilde{\boldsymbol{m}}_1 = \{\widetilde{m}_1^{(1)}, \widetilde{m}_1^{(2)}, \widetilde{m}_1^{(3)}\}^T = \{1, 2, 3\}^T$ (Figure 4C). Based on the introduced notation, the procedure described in Steps 1 to 5 is formally given in Algorithm 1.

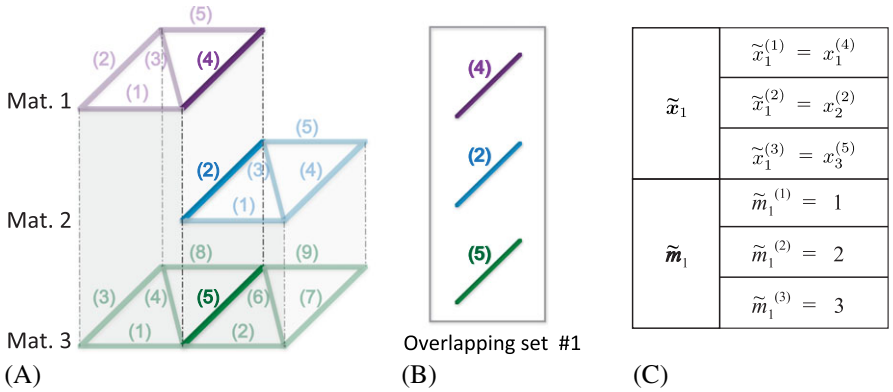

$$\begin{array}{|l|l|}\hline \tilde{\boldsymbol{x}}_1 & \tilde{x}_1^{(1)} = x_1^{(4)} \\ & \tilde{x}_1^{(2)} = x_2^{(2)} \\ & \tilde{x}_1^{(3)} = x_3^{(5)} \\ \hline \tilde{\boldsymbol{m}}_1 & \tilde{m}_1^{(1)} = 1 \\ & \tilde{m}_1^{(2)} = 2 \\ & \tilde{m}_1^{(3)} = 3 \\ \hline \end{array}$$

FIGURE 4 Demonstration of the overlapping of 3 materials and the corresponding notation. (A) A design consisting of overlapping connectivities; (B) overlapping connectivity set #1 containing the fourth member of *Material 1*, the second member of *Material 2*, and the fifth member of *Material 3*; (C) corresponding notation [Colour figure can be viewed at wileyonlinelibrary.com]

Algorithm 1 Algorithm to select a single preferred material

Input: $\boldsymbol{x}_1, \ldots, \boldsymbol{x}_m$, α_{select}
Detect p sets of members with more than one material selection, $\tilde{\boldsymbol{x}}_1, \ldots, \tilde{\boldsymbol{x}}_p$.
for $j = 0, 1, \ldots, p$ **do**
  Detect the member i^* with the largest strain energy per unit length among $\tilde{\boldsymbol{x}}_j$ such that

$$\tilde{x}_j^{(i^*)} \Psi_{\tilde{m}_j^{(i^*)}} = \max\left(\tilde{x}_j^{(1)} \Psi_{\tilde{m}_j^{(1)}}, \ldots, \tilde{x}_j^{(n)} \Psi_{\tilde{m}_j^{(n)}}\right), \tag{21}$$

  where n indicates the length of vector $\tilde{\boldsymbol{x}}_j$.
  if $\tilde{x}_j^{(i^*)} / \max\left(\boldsymbol{x}_{\tilde{m}_j^{(i^*)}}\right) \geq \alpha_{\text{select}}$ **then**

$$\tilde{x}_j^{(i)} = \begin{cases} \tilde{x}_j^{(i)}, & \text{if} \quad i = i^* \\ 0, & otherwise. \end{cases} \qquad i = 1, \ldots, n \tag{22}$$

  end if
end for
Update $\boldsymbol{x}_1, \ldots, \boldsymbol{x}_m$ based on corresponding components of $\tilde{\boldsymbol{x}}_1, \ldots, \tilde{\boldsymbol{x}}_p$
Output: New $\boldsymbol{x}_1, \ldots, \boldsymbol{x}_m$

Algorithm 1 describes the procedure of selecting a single material from each overlapping connectivity at each optimization step. Incorporating Algorithm 1 in the optimization process, the entire implementation is described in Algorithm 2. In Section 6.1, we include studies that demonstrate influences of the main algorithmic parameters (N_{select} and α_{select}) on the final topologies and objective values.

We remark that the above-presented material selection algorithm can also be applied with the discrete filter scheme[22,23] to control the resolution of the final topology and improve the computational efficiency. Typically, the discrete filter starts at the initial step of the optimization process. However, in this case, the discrete filter may remove the potential members to redistribute the removed overlapping materials. Zhang et al[22] indicated that the discrete filter can remove up to 99% of the members in the first few optimization steps after the filter is applied, which may significantly reduce the space of potential members to redistribute the removed overlapping materials (when we start to apply Algorithm 1 after N_{select} steps). Thus, in the optimization algorithm, we propose to apply the discrete filter after N_{filter} optimization steps, where $N_{\text{filter}} > N_{\text{select}}$ is a prescribed parameter.

Algorithm 2 Multimaterial topology optimization with the proposed algorithm that selects a single preferred material

Initialize: $\boldsymbol{x}_1^0, \ldots, \boldsymbol{x}_m^0$, $\text{iter}_{\max}$, tol_{opt}, N_{select}, N_{filter}
for $k = 0, 1, \ldots, \text{iter}_{\max}$ **do**
  Solve: $\boldsymbol{u}\left(\boldsymbol{x}_1^k, \ldots, \boldsymbol{x}_m^k\right) = \arg\min_{\boldsymbol{u}} \left[\Pi\left(\boldsymbol{x}_1^k, \ldots, \boldsymbol{x}_m^k, \boldsymbol{u}\right)\right]$
  Compute: $J\left(\boldsymbol{x}_1^k, \ldots, \boldsymbol{x}_m^k\right), g^j\left(\boldsymbol{x}_1^k, \ldots, \boldsymbol{x}_m^k\right), \partial J\left(\boldsymbol{x}_1^k, \ldots, \boldsymbol{x}_m^k\right)/\partial x_i^{(e)}$, and $\partial g^j\left(\boldsymbol{x}_1^k, \ldots, \boldsymbol{x}_m^k\right)/\partial x_i^{(e)}$
  for $j = 1, 2, \ldots, nc$ **do**
    Compute ϕ_{V*}^j by solving Equation (18)
    Update $x_i^{(e),k+1} = Q_i^{(e),k}\left(\phi_V^{j*}\right), \quad \forall i \in \mathcal{G}^j$ according to Equation (20)
  end for
  if $k \geq N_{\text{select}}$ **then**
    Apply Algorithm 1 to the sets of overlapping members
  if $k \geq N_{\text{filter}}$
    Apply discrete filter according to Equation (7)
  end if
  if $\max\left(||\boldsymbol{x}_1^{k+1} - \boldsymbol{x}_1^k||_\infty, \ldots, ||\boldsymbol{x}_m^{k+1} - \boldsymbol{x}_m^k||_\infty\right) < \text{tol}_{\text{opt}}$ and $k > N_{\text{select}}$ **then**
    quit
  end if
end for
Remove aligned nodes
Plot final topology

6 | EXAMPLES

In this section, we provide several numerical examples to demonstrate the proposed material selection algorithm in the multimaterial topology optimization using the GSM. Example 1 investigates the main parameters of the selecting algorithm, ie, N_{select} and α_{select}. Example 2 demonstrates the selecting algorithm using 4 Ogden-based materials and compares the optimized results to the multimaterial case without the selecting algorithm. Using 1 linear material model and 2 bilinear material models, Example 3 illustrates the selecting algorithm in a simplified bridge design. The last example shows the application of the proposed multimaterial formulation to a 3-dimensional cantilever beam design.

We generate nonoverlapped (within the same material layer) initial GS using the collision zone technique by Zegard and Paulino[29,30] and plot final topologies in 3D using the program GRAND3.[30] For all results in the GSM, we remove aligned nodes and floating members and check the final topologies to ensure that they are at global equilibrium. A detailed explanation can be found in the work of Zhang et al.[31] It is worth noting that we do not verify the instability of the members because the issue of stability is beyond the scope of this work. The nonlinear solution scheme is based on a Newton-Raphson approach with line search (see the work of Zhang et al[22] for a detailed explanation). For all the examples, the discrete filter is used during the optimization process to obtain valid structures and improve computational efficiency.

For the constitutive models of the numerical example, we employ a linear model, a bilinear model, and a (hyperelastic) Ogden-based[20] model, which allows a varied control of constitutive relationships and has the capability to reproduce a variety of hyperelastic models. For details of the constitutive models and strain energy density functions that form the basis of the structural analysis, readers are referred to the studies of Ramos Jr and Paulino[21] and Zhang et al.[22]

Consistent units are implied throughout, and examples have the initial tangent modulus, ie, $E_0 = 7 \times 10^7$, unless otherwise stated; stopping criterion, ie, $\text{tol}_{\text{opt}} = 10^{-9}$; move value, ie, $move = 10^4 x^0$, where x^0 is the initial guess of the design variables; and initial damping factor for the ZPR update scheme, ie, $\eta = 0.5$. Subsequent damping factors are updated according to the scheme provided by the study of Groenwold and Etman.[28] The upper bound for the design variable is defined by $x_{\max} = 10^4 x^0$. *All examples are solved using the ZPR design variable update scheme described in Section* 4*, and all cases that enforce the selection of a single material employ the material selection algorithm described in Algorithm* 1.

6.1 | Example 1: parametric study using a cantilever beam

In this example, we demonstrate the effectiveness of the proposed material selection algorithm and investigate the main parameters, ie, N_{select} and α_{select}. The design domain ($L = 2, P = 1000$) and material models are shown in Figures 5A and 5B. Three materials share the entire domain, as shown in Figure 5C. Three layers (one for each material) of identical full-level initial GS (based on a 8×6 discretization) with a total of 3,702 members and 63 nodes are used. The total prescribed maximum volume takes the following value: $V_{\max} = 0.024$. Each material is associated with an individual volume constraint ($nc = 3$), as shown in Table 2.

To investigate the impact of the step number to initiate the selection algorithm (Algorithm 1), ie, N_{select}, we choose $N_{\text{select}} = 1, 2, 20, 40, 60, 100, 200, 300, 360$. In all the cases, $\alpha_{\text{select}} = 0.05$, $\alpha_{\text{f}} = 0.005$, and we initiate the discrete filter at optimization step 365, ie, $N_{\text{filter}} = 365$. Figure 6 shows the optimized objective function value for each N_{select} and the final topologies from representative N_{select}. For comparison purposes, the optimized objective value and the final topology obtained from the multimaterial formulation without the selection algorithm are also plotted in Figure 6. The data are summarized in Table 2.

Several observations can be made based on Figure 6 and Table 2. When the selection algorithm is not used, the final topology has the smallest objective function value and every member contains more than one material (18 overlapping connectivities). The cases applying the selection algorithm with $\alpha_{\text{select}} = 0.05$ lead to final topologies with single-material

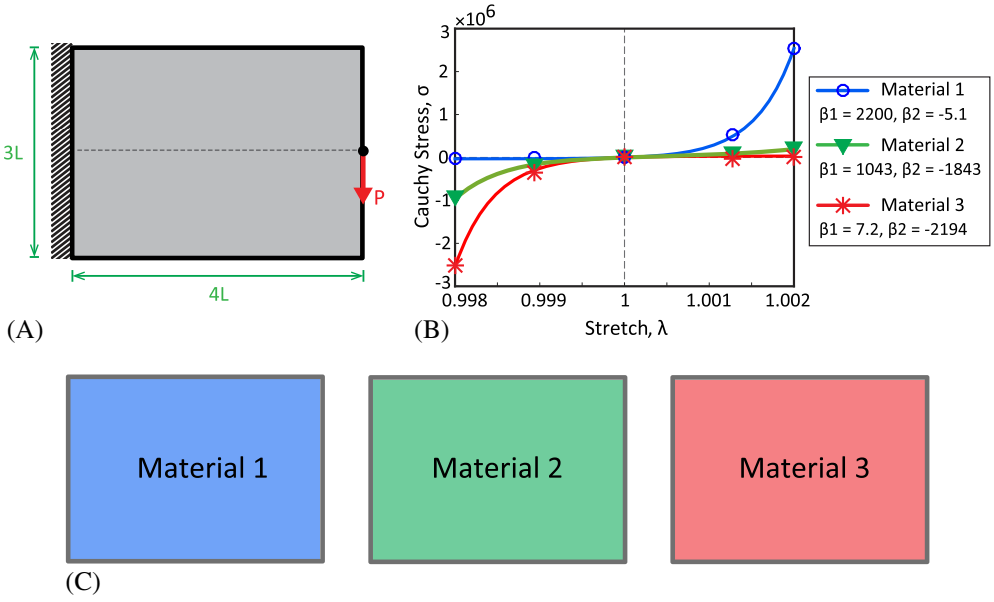

FIGURE 5 Example 1: Cantilever beam with 3 Ogden-based materials. (A) Design domain ($L = 2, P = 1000$); (B) material models, ie, 3 Ogden-based materials; (C) initial material distribution, ie, the 3 materials share the entire domain [Colour figure can be viewed at wileyonlinelibrary.com]

TABLE 2 Numerical information for Example 1 (see Figures 5, 6, and 7)

Study of N_{select}				Study of α_{select}			
N_{select}	α_{select}	$J(x_i^*)$	No. of Overlapping Connectivities	N_{select}	α_{select}	$J(x_i^*)$	No. of Overlapping Connectivities
1		27.954			0.00	27.604	0
2		27.501			0.01	27.487	0
20		27.498			0.05	27.475	0
40		27.487			0.10	27.452	0
60	0.05	27.475	0	60	0.30	27.432	4
100		27.452			0.50	27.432	12
200		27.452			0.75	27.432	12
300		27.452			1.00	27.432	18
360		27.452					

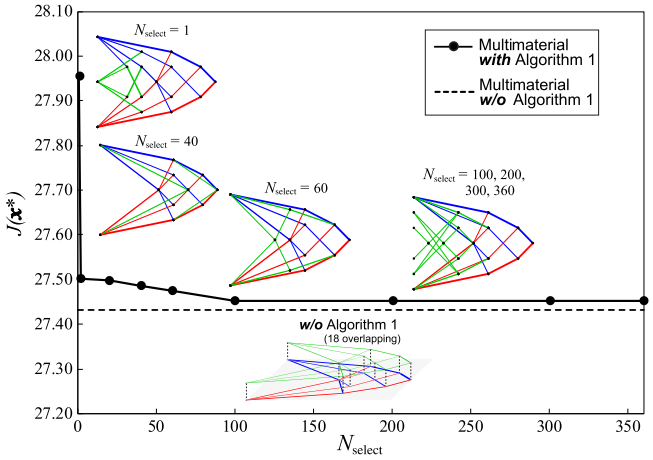

FIGURE 6 Example 1: study of the step number to initiate the selecting algorithm, ie, N_{select}, ($N_{\text{select}} = 1, 2, 20, 40, 60, 100, 200, 300, 360$) versus the resulting optimized objective value. The final topologies (from representative cases) are included. Other parameters: $\alpha_{\text{select}} = 0.05$, $\alpha_{\text{f}} = 0.005$, and $N_{\text{filter}} = 365$ [Colour figure can be viewed at wileyonlinelibrary.com]

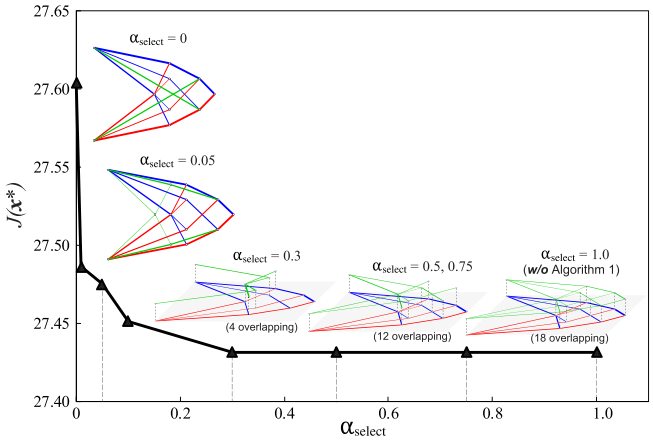

FIGURE 7 Example 1: influence of α_{select} on the optimization results, ie, α_{select}, ($\alpha_{\text{select}} = 0, 0.01, 0.05, 0.1, 0.3, 0.5, 0.75, 1$) versus the resulting optimized objective value. The final topologies (from representative cases) are included. Other parameters: $N_{\text{select}} = 60$, $\alpha_f = 0.005$, and $N_{\text{filter}} = 365$ [Colour figure can be viewed at wileyonlinelibrary.com]

members and no overlapping connectivity for all N_{select} values. The later we initiate the selection algorithm, the lower final objective function value obtained; in addition, initiating later tends to result in more complex structures and a higher computational time. Moreover, for the cases with $N_{\text{select}} \geq 100$, ie, $N_{\text{select}} = 100, 200, 300, 360$, we obtain identical $J(\boldsymbol{x}_i^*)$ values and optimized structures. These observations suggest that initiating the selection algorithm early in the optimization process provides access to various solutions, whereas initiating it later in the optimization results in a similar solution. By varying N_{select} to initiate the selection algorithm, various optimized structures with similar $J(\boldsymbol{x}_i^*)$ can be obtained, all without overlapping connectivity (ie, each member contains a single material).

The next study demonstrates the effect of α_{select} on the optimization results. The threshold α_{select} determines if the material selection algorithm is performed on each connectivity. The value of α_{select} varies between $0 \leq \alpha_{\text{select}} \leq 1$, where $\alpha_{\text{select}} = 0$ corresponds to applying the selection algorithm to all the overlapping connectivities, and $\alpha_{\text{select}} = 1$ corresponds to never applying the selection algorithm. We choose $\alpha_{\text{select}} = 0, 0.01, 0.05, 0.1, 0.3, 0.5, 0.75, 1$. In this study, $N_{\text{select}} = 60$, $\alpha_f = 0.005$, and $N_{\text{filter}} = 365$. Figure 7 shows the optimized objective function value for each α_{select} and the final topologies from representative α_{select}. The data are summarized in Table 2.

We observe that a larger α_{select} (more conservative, closer to 1) leads to a lower optimized objective function value. However, if $\alpha_{\text{select}} \geq 0.3$, the resulting structures contain members with more than one material. On the other hand, smaller threshold values (more drastic), eg, $\alpha_{\text{select}} \leq 0.1$, lead to structures with a single preferred material at every subdomain. The threshold α_{select}, allows the designer to choose the complexity of the design and whether the material profile contains

either single materials or composite materials. For the examples in the remainder of this paper, we choose $\alpha_{select} = 0.05$ for the selection algorithm unless otherwise stated to effectively and efficiently select a single material among multiple materials.

6.2 | Example 2: opposite loads in a simply supported rectangular domain

This example demonstrates the selection algorithm using 4 Ogden-based materials in 2D and compares the optimized results with the multimaterial case without the material selection algorithm (ie, no control on the number of the materials selected for each connectivity). The design domain with load and boundary conditions ($L = 10, P = 1000$) and material models are shown in Figures 8A and 8B. Four materials share the entire domain (Figure 8C). Four layers (1 for each material) of identical level-10 initial GS (based on a 30×10 grid) with a total of 78 528 members and 341 nodes are used. The total prescribed maximum volume takes the following value, ie, $V_{max} = 0.15$. Each material is associated with an individual volume constraint ($nc = 4$), as shown in Table 3. For the case employing the selection algorithm, we start to select the preferred material at $N_{select} = 30$ with the ratio $\alpha_{select} = 0.05$. For both cases (with and without the selecting algorithm), the filter parameters are $\alpha_f = 0.001$ and $N_{filter} = 100$.

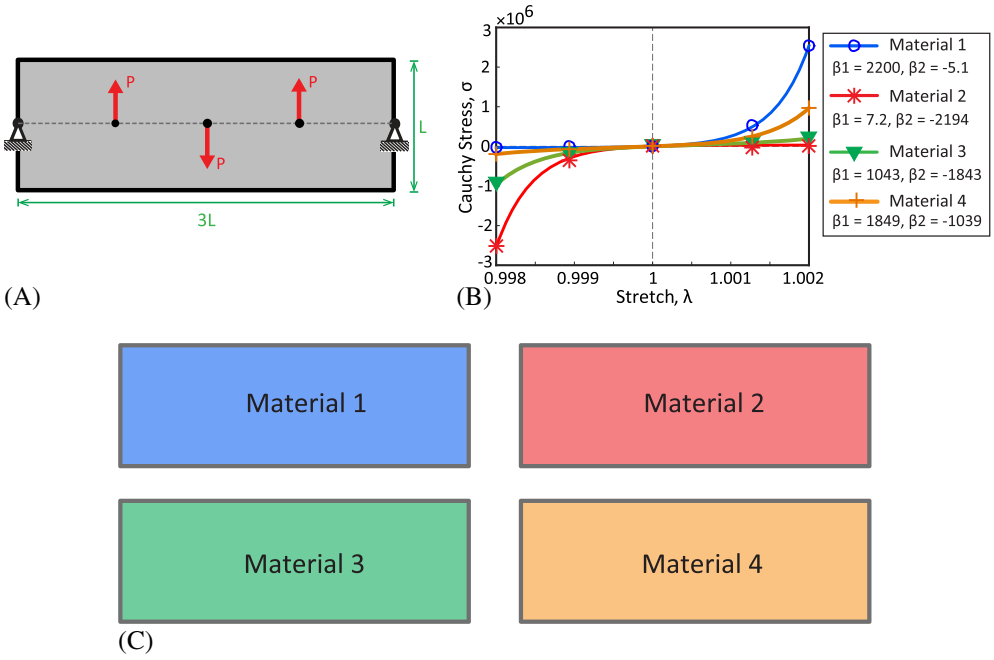

FIGURE 8 Example 2: opposite loads in a simply supported rectangular domain. (A) Design domain ($L = 10, P = 1000$); (B) material models, ie, 4 Ogden-based materials; (C) initial material distribution, ie, 4 materials share the entire domain [Colour figure can be viewed at wileyonlinelibrary.com]

TABLE 3 Numerical information for Example 1 (see Figures 8, 9, and 10)

2D Cases	$J(x_i^*)$	Material β_1	Material β_2	Volume Constraint, V^j_{max}	No. of Elements	No. of Overlapping connectivities
4 materials		2200.3	−5.1	$0.4V_{max}$	33	
	27.510	7.2	−2194.0	$0.4V_{max}$	33	66
(standard)		1043.3	−1843.1	$0.1V_{max}$	33	
		1848.8	−1039.2	$0.1V_{max}$	33	
4 materials		2200.3	−5.1	$0.4V_{max}$	24	
	27.562	7.2	−2194.0	$0.4V_{max}$	24	0
(**Algorithm 1**)		1043.3	−1843.1	$0.1V_{max}$	16	
		1848.8	−1039.2	$0.1V_{max}$	16	

Abbreviations: 2D, 2-dimensional.

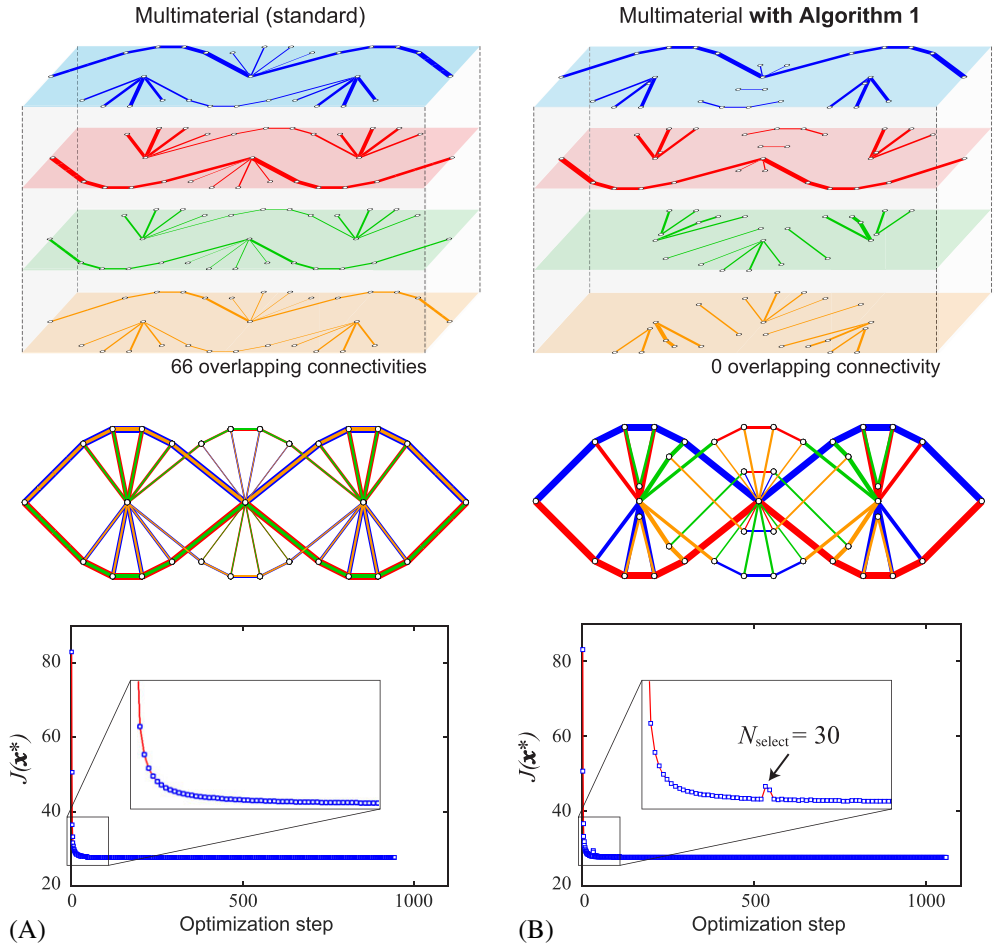

FIGURE 9 Example 2: opposite loads in a simply supported rectangular domain. (A) Optimized structure and convergence plot without the proposed selection algorithm ($\alpha_f = 0.001$, $N_{\text{filter}} = 100$) that contains 66 overlapped connectivities (before removing aligned nodes); (B) optimized structure and convergence plot with the proposed selection algorithm ($\alpha_{\text{select}} = 0.05$, $N_{\text{select}} = 30$, $\alpha_f = 0.001$, and $N_{\text{filter}} = 100$) that selects a single material among multiple materials—no overlapping connectivity is observed in the final design [Colour figure can be viewed at wileyonlinelibrary.com]

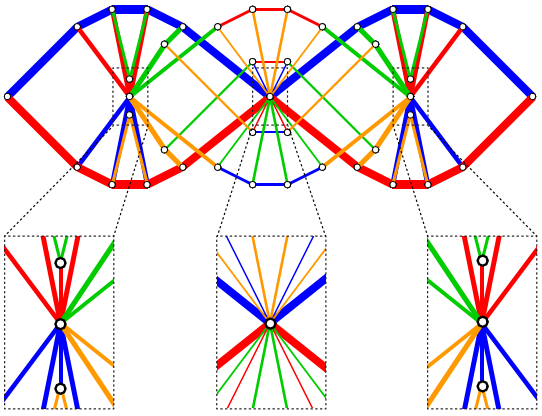

FIGURE 10 Example 2: Zoom-in regions of the optimized structure obtained from the proposed selection algorithm. No overlapping connectivity is observed in the final design [Colour figure can be viewed at wileyonlinelibrary.com]

Both the optimized structures and convergence plots for the cases with and without enforcement of the selection of one material are shown in Figure 9A,B. The associated numerical information is summarized in Table 3. An optimized structure with every member containing more than one material (66 overlapping connectivities in total before removing aligned nodes) is obtained in the case without the selection algorithm. *Material 1* and *Material 4* are selected for the

members in tension; *Material 2* and *Material 3* are selected for the members in compression. As shown in Figure 10, the multimaterial framework with the selection algorithm leads to a structure in which members contain at most one material (no overlapping connectivity) and a slightly larger objective value. In addition, we observe an increase in the objective function at the step where the selection algorithm is initiated, ie, $N_{\text{select}} = 30$. This corresponds to the removal of certain overlapping members, as shown in Figure 9B. The convergence of the objective function at other steps is smooth.

6.3 | Example 3: long-span bridge design using linear and bilinear materials

This multimaterial bridge example illustrates the material selection algorithm using 1 linear material model and 2 bilinear material models. The design domain (with load and boundary conditions) is shown in Figure 11A. Two bilinear materials and 1 linear material are used and share the entire domain, as shown in Figure 11B,C, leading to 3 identical layers of full-level initial GS (based on an 18×7 grid) with 21 249 nonoverlapping members and 152 nodes. Each material is assigned to an individual volume constraint (see Table 4). Here, we optimize the bridge problem with and without the proposed algorithm that removes overlapped members from multiple materials. In the case employing the selection algorithm, we choose $N_{\text{select}} = 30$ and $\alpha_{\text{select}} = 0.05$. For both cases (with and without the selection algorithm), the filter parameters are $\alpha_f = 0.001$ and $N_{\text{filter}} = 100$.

The optimized structures for the case with and without the enforcement of the selection of one material are shown in Figure 12A,B. The associated numerical information is summarized in Table 4. The results verify the proposed algorithm that selects a single preferred material. In the optimized structure, we observe that the selection of more than one material for some truss members (ie, overlapping of truss members from different materials) occurs in the case without the proposed selection algorithm. This leads to an optimized bridge design that contains 25 overlapped composite members and a smaller objective value. This optimized structure contains members with *composite* materials, ie, *Material 2* and *Material 3* are selected for the members in compression. On the other hand, the case with the proposed algorithm leads to the result containing no overlapped members and a larger objective value.

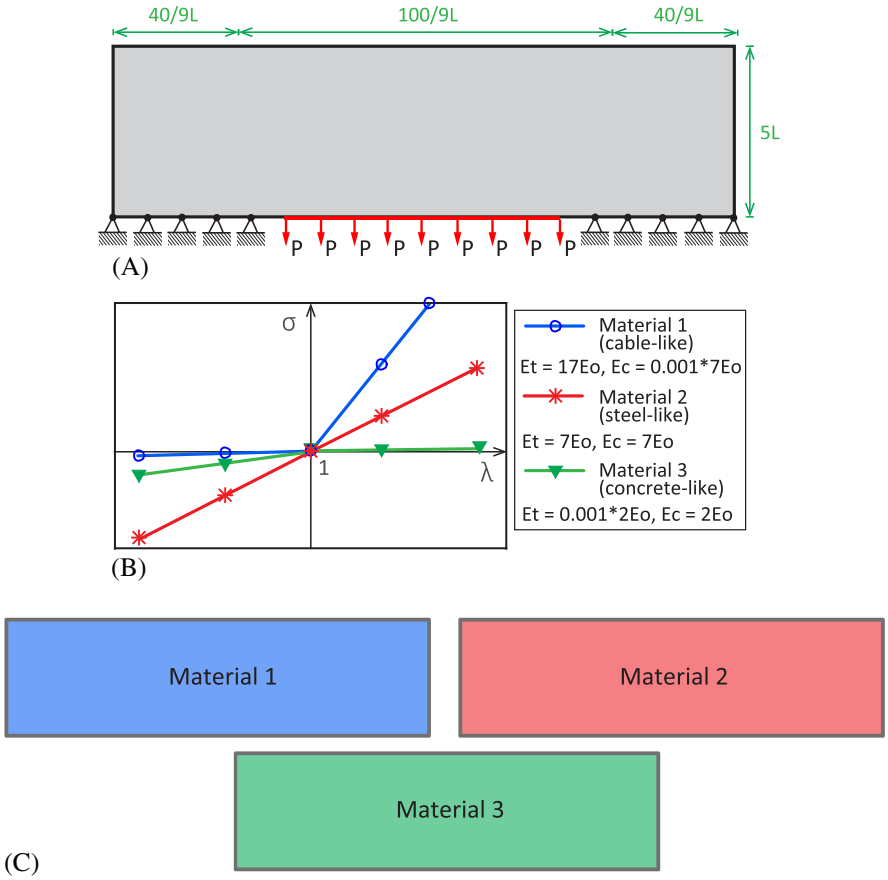

FIGURE 11 Example 3: Multimaterial bridge design. (A) Design domain; (B) material models, ie, 2 bilinear materials and 1 linear material; (C) initial material distribution for each material [Colour figure can be viewed at wileyonlinelibrary.com]

TABLE 4 Numerical information for Example 3 (see Figures 11 and 12), ie, $E_o = 10^7$

2D Cases	$J(x_i^*)$	Material E_t	Material E_c	Volume Constraint, V^j_{max}	No. of Elements	No. of Overlapping Connectivities
3 materials (standard)	20.920	$17E_o$	$0.001E_o$	$0.4V_{max}$	35	25
		$7E_o$	$7E_o$	$0.1V_{max}$	25	
		$0.002E_o$	$2E_o$	$0.5V_{max}$	25	
3 materials (**Algorithm 1**)	21.417	$17E_o$	$0.001E_o$	$0.4V_{max}$	42	0
		$7E_o$	$7E_o$	$0.1V_{max}$	11	
		$0.002E_o$	$2E_o$	$0.5V_{max}$	16	

Abbreviations: 2D, 2-dimensional.

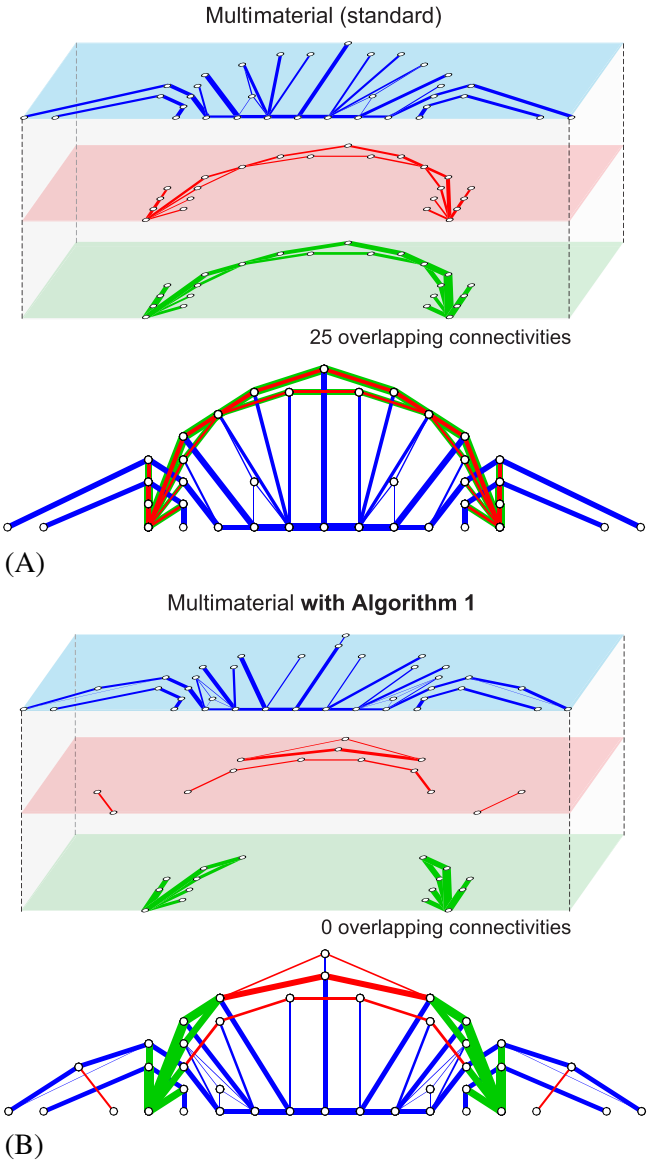

FIGURE 12 Example 3: Multimaterial bridge design. (A) Optimized bridge design without the selection algorithm that contains 25 overlapped connectivities ($\alpha_f = 0.001$, $N_{filter} = 100$); (B) optimized bridge design with the proposed selection algorithm that selects a single material among multiple materials at each subdomain ($\alpha_{select} = 0.05$, $N_{select} = 30$, $\alpha_f = 0.001$, $N_{filter} = 100$) [Colour figure can be viewed at wileyonlinelibrary.com]

6.4 | Example 4: 3D cantilever beam

Using a combination of different materials, we apply the proposed material selection algorithm to a 3D cantilever beam. The geometry, load, and boundary conditions ($L = 1, P = 60$) are shown in Figure 13A. To obtain constructible structures, we use a $6 \times 2 \times 2$ discretization (with a level-3 GS) for the domain containing 5 000 members and 63 nodes. We perform optimization with 4 Ogden-based materials, as shown in Figure 13B, and these 4 materials share the entire domain. Four volume constraints are used ($nc = 4$). The total prescribed maximum volume takes the following value: $V_{\max} = 0.024$. For the selection algorithm, we choose $N_{\text{select}} = 30$ and $\alpha_{\text{select}} = 0.05$ and initiate the filter at $N_{\text{filter}} = 60$. In addition to a small

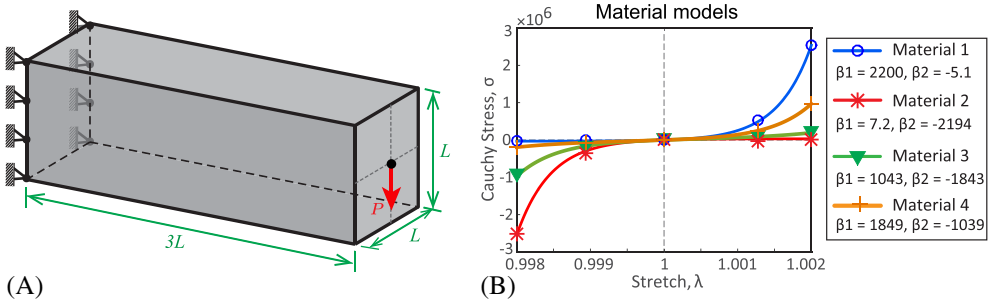

FIGURE 13 Three-dimensional multimaterial cantilever beam design. (A) Design domain discretized using a $6 \times 2 \times 2$ grid; (B) material models, ie, 4 Ogden-based materials [Colour figure can be viewed at wileyonlinelibrary.com]

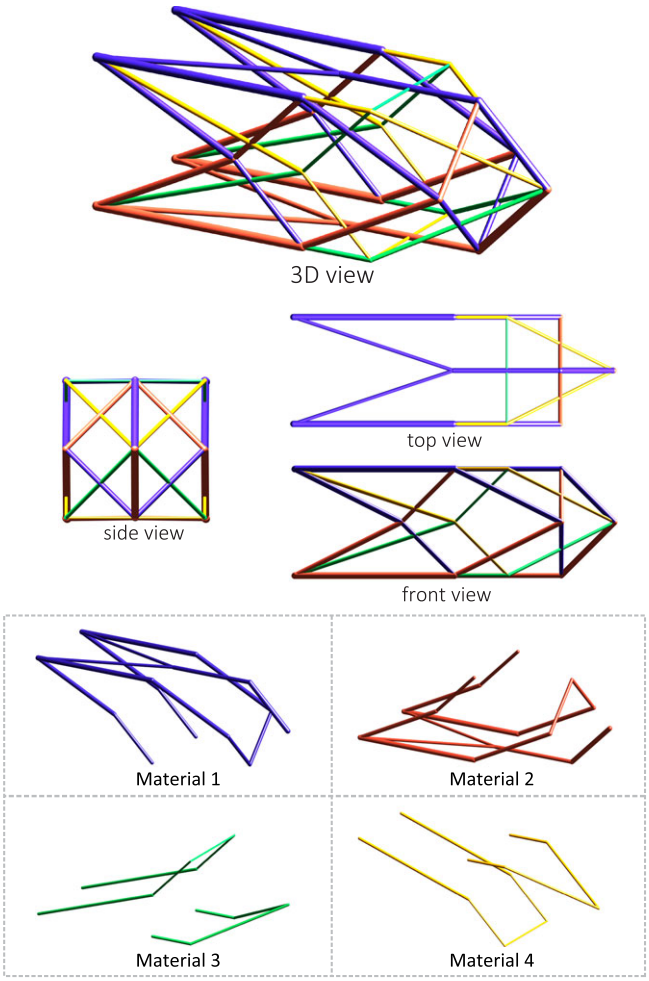

FIGURE 14 The optimized structure for the 3-dimensional (3D) cantilever design with the selection algorithm (enforcing the selection of one material) with $\alpha_{\text{select}} = 0.05$, $N_{\text{select}} = 30$, $\alpha_f = 0.0001$ (optimization), $\alpha_f = 0.01$ (end), and $N_{\text{filter}} = 30$. No overlapping connectivity is observed in the final design

TABLE 5 Numerical information for Example 4 (see Figures 13 and 14)

3D Case	$J(x_i^*)$	Material		Volume constraint, V^j_{max}	No. of Elements	No. of Overlapping connectivities
		β_1	β_2			
4 materials		2200.3	−5.1	$0.4V_{max}$	14	
	51.01	7.2	−2194.0	$0.4V_{max}$	14	0
(**Algorithm 1**)		1043.3	−1843.1	$0.1V_{max}$	9	
		1848.8	−1039.2	$0.1V_{max}$	9	

Abbreviations: 3D, 3-dimensional.

filter ($\alpha_f = 10^{-4}$) used throughout the optimization, we use a larger filter ($\alpha_f = 10^{-2}$) in the final step of the optimization to control the resolution of the final topology.

The optimized structure for the case with enforcing the selection of one material is shown in Figure 14. The associated numerical information is summarized in Table 5. The result indicates that the multimaterial framework with the material selection algorithm can also effectively produce a structure with single-material members (ie, no overlapping connectivity) in 3 dimensions.

7 | CONCLUDING REMARKS

In this paper, we have investigated the issue of selecting more than one material that occurs in multimaterial topology optimization in the context of truss layout optimization. We examine the conditions (that need to be satisfied simultaneously) in which the selection of multiple materials on a certain connectivity occurs, ie, more than one material sharing the domain, each of them associated with an individual volume constraint, and one material being stronger at least within a certain range of stretch values. To ensure the selection of a single material at each subdomain, we propose an algorithm (Algorithm 1) that selects a preferred material among multiple materials based on the evaluation of both the strain energy and the cross-sectional area of each member. This algorithm actively and iteratively selects materials to ensure the selection of a single material for each member. The ZPR design variable update scheme for multimaterial optimization is employed, and we provide an alternative derivation of this update scheme using the KKT conditions.

Using combinations of Ogden-based, bilinear, and linear materials, we verify the proposed selection algorithm and compare the results to the ones obtained without using the selection algorithm. We also demonstrate that the algorithmic parameters, ie, the step number to initiate and the threshold of the selection algorithm, allow the designers to control both the complexity of the final design, as well as the final material profile to use either single materials or composite materials. We conclude that the material selection algorithm for multimaterial topology optimization is efficient and effective for selecting a single preferred material per overlapping set.

ACKNOWLEDGEMENTS

The authors acknowledge the financial support from the US National Science Foundation (NSF) under the project #1559594 (formerly #1335160) and from the Laboratory of Scientific Computing and Visualization (LCCV) Technology Center at the Federal University of Alagoas (UFAL). We are also grateful for the endowment provided by the Raymond Allen Jones Chair at the Georgia Institute of Technology. The information provided in this paper is the sole opinion of the authors and does not necessarily reflect the views of the sponsoring agencies.

ORCID

Xiaojia Shelly Zhang https://orcid.org/0000-0003-4878-8637
Glaucio H. Paulino http://orcid.org/0000-0002-3493-6857

REFERENCES

1. Bendsøe MP, Sigmund O. Material interpolation schemes in topology optimization. *Arch Appl Mech*. 1999;69(9-10):635-654.
2. Sigmund O, Torquato S. Design of materials with extreme thermal expansion using a three-phase topology optimization method. *J Mech Phys Solids*. 1997;45(6):1037-1067.
3. Gibiansky LV, Sigmund O. Multiphase composites with extremal bulk modulus. *J Mech Phys Solids*. 2000;48(3):461-498.

4. Hvejsel CF, Lund E. Material interpolation schemes for unified topology and multi-material optimization. *Struct Multidiscip Optim*. 2011;43(6):811-825.
5. Stegmann J, Lund E. Discrete material optimization of general composite shell structures. *Int J Numer Methods Eng*. 2005;62(14):2009-2027.
6. Yin L, Ananthasuresh G. Topology optimization of compliant mechanisms with multiple materials using a peak function material interpolation scheme. *Struct Multidiscip Optim*. 2001;23(1):49-62.
7. Wallin M, Ivarsson N, Ristinmaa M. Large strain phase-field-based multi-material topology optimization. *Int J Numer Methods Eng*. 2015;104(9):887-904.
8. Zhou S, Wang MY. Multimaterial structural topology optimization with a generalized Cahn–Hilliard model of multiphase transition. *Struct Multidiscip Optim*. 2007;33(2):89-111.
9. Tavakoli R, Mohseni SM. Alternating active-phase algorithm for multimaterial topology optimization problems: a 115-line MATLAB implementation. *Struct Multidiscip Optim*. 2014;49(4):621-642.
10. Wang MY, Wang X. Color level sets: a multi-phase method for structural topology optimization with multiple materials. *Comput Methods Appl Mech Eng*. 2004;193(6):469-496.
11. Wang MY, Wang X. A level-set based variational method for design and optimization of heterogeneous objects. *Comput Aided Des*. 2005;37(3):321-337.
12. Wang MY, Chen S, Wang X, Mei Y. Design of multimaterial compliant mechanisms using level-set methods. *J Mech Des*. 2005;127(5):941-956.
13. Mei Y, Wang X. A level set method for structural topology optimization with multi-constraints and multi-materials. *Acta Mech Sinica*. 2004;20(5):507-518.
14. Gaynor A, Guest J, Moen C. Reinforced concrete force visualization and design using bilinear truss-continuum topology optimization. *J Struct Eng*. 2012;139(4):607-618.
15. Victoria M, Querin OM, Martí P. Generation of strut-and-tie models by topology design using different material properties in tension and compression. *Struct Multidiscip Optim*. 2011;44(2):247-258.
16. Bogomolny M, Amir O. Conceptual design of reinforced concrete structures using topology optimization with elastoplastic material modeling. *Int J Numer Methods Eng*. 2012;90(13):1578-1597.
17. Amir O, Sigmund O. Reinforcement layout design for concrete structures based on continuum damage and truss topology optimization. *Struct Multidiscip Optim*. 2013;47(2):157-174.
18. Zegard T, Paulino GH. Truss layout optimization within a continuum. *Struct Multidiscip Optim*. 2013;48(1):1-16.
19. Zhang XS, Paulino GH, Ramos Jr AS. Multi-material topology optimization with multiple volume constraints: a ground structure approach involving material nonlinearity. *Struct Multidiscip Optim*. 2017:1-22. https://doi.org/10.1007/s00158-017-1768-3
20. Ogden RW. *Non-Linear Elastic Deformations*. Long Island, NY: Dover Publications Inc; 1984.
21. Ramos Jr AS, Paulino GH. Convex topology optimization for hyperelastic trusses based on the ground-structure approach. *Struct Multidiscip Optim*. 2015;51(2):287-304.
22. Zhang X, Ramos Jr AS, Paulino GH. Material nonlinear topology design using the ground structure method with a discrete filter scheme. *Struct Multidiscip Optim*. 2017;55(6):2045-2072.
23. Ramos Jr AS , Paulino GH. Filtering structures out of ground structures – a discrete filtering tool for structural design optimization. *Struct Multidiscip Optim*. 2016;54(1):95-116.
24. Tikhonov A, Arsenin V. *Methods For Solving Ill-Posed Problems*. New York, NY: Wiley; 1977.
25. Felippa C. Newton method: General control and variants. Lecture Notes nd. prefix. http://www.colorado.edu/engineering/cas/courses.d/NFEM.d/NFEM.Ch26.d/NFEM.Ch26.pdf
26. Talischi C, Paulino GH. An operator splitting algorithm for Tikhonov-regularized topology optimization. *Comput Methods Appl Mech Eng*. 2013;253:599-608.
27. Christensen P, Klarbring A. *An Introduction To Structural Optimization*. Linköping, Sweden: Springer Science & Business Media; 2009.
28. Groenwold AA, Etman L. On the equivalence of optimality criterion and sequential approximate optimization methods in the classical topology layout problem. *Int J Numer Methods Eng*. 2008;73(3):297-316.
29. Zegard T, Paulino GH. GRAND – Ground structure based topology optimization for arbitrary 2D domains using MATLAB. *Struct Multidiscip Optim*. 2014;50(5):861-882.
30. Zegard T, Paulino GH. GRAND3 – Ground structure based topology optimization for arbitrary 3D domains using MATLAB. *Struct Multidiscip Optim*. 2015;52(6):1161-1184.
31. Zhang X, Maheshwari S, Ramos JrAS, Paulino GH. Macroelement and macropatch approaches to structural topology optimization using the ground structure method. *ASCE J Struct Eng*. 2016;142(11):04016 090-1-14. https://doi.org/10.1061/(ASCE)ST.1943-541X.0001524

How to cite this article: Zhang XS, Paulino GH, Ramos Jr AS. Multimaterial topology optimization with multiple volume constraints: Combining the ZPR update with a ground-structure algorithm to select a single material per overlapping set. *Int J Numer Methods Eng*. 2018;114:1053–1073. https://doi.org/10.1002/nme.5736

APPENDIX: NOMENCLATURE

α	Exponent coefficient used in the ZPR model to define $\boldsymbol{y}_i$
α_f	Filter value
α_{select}	Threshold of the selecting algorithm (Algorithm 1)
η	Damping factor in the ZPR model
Γ	Tikhonov regularization parameter
γ_i, β_i	Ogden material parameters
λ	Linearized stretch
λ_i	Principal stretches
$\mathcal{G}^j$	The set of material indices associated with the jth volume constraint in the ZPR model
$\widetilde{m}_j$	Vector of material indices for the jth overlapping set
$\widetilde{x}_j$	Vector containing all the design variables in the jth overlapping set
$\bar{\boldsymbol{x}}_i$	Vector of filtered design variables (cross-sectional areas) with material i
$\bar{x}_i^{(e)}$	Filtered cross-sectional area of member e with material i
ϕ_V^j	Lagrange multiplier introduced for the jth volume constraint in the ZPR model
ϕ_V^{j*}	The optimal Lagrange multiplier introduced for the jth volume constraint of the ZPR model
Π	Total potential energy
$\Psi_i^{(e)}$	Strain energy density function of member e with material i
Ψ_{Bi}	Bilinear strain energy density function
Ψ_{OG}	Ogden strain energy density function
$b_i(\boldsymbol{x}_1^k, \ldots, \boldsymbol{x}_m^k)$	Sensitivity vector of the objective function J with respect to $\boldsymbol{y}_i$ evaluated at the kth step in the ZPR model
$\boldsymbol{f}$	External force vector
$\boldsymbol{L}_i$	Vector of member length for material i
$\boldsymbol{N}$	Unit directional vector of a given truss member
$\boldsymbol{u}$	Displacement vector
$\boldsymbol{u}_p$, $\boldsymbol{u}_q$	Displacements of nodes p and q for a given truss member
$\boldsymbol{x}_i$	Vector of design variables (cross-sectional areas) with material i
$\boldsymbol{y}_i$	Vector of intervening variables with material i
E_0	Initial tangent modulus (Young's modulus)
g^j	The jth volume constraint in the ZPR model
J	Objective function
J^k	Approximated objective function in the subproblem at optimization step k
$L_i^{(e)}$	Length of truss member e with material i
M	Ogden material parameter
m	Total number of materials
M_i	Number of truss members in material i
$move$	Prescribed move limit in the ZPR model
N_{select}	Step number to initiate the selecting algorithm (Algorithm 1)
nc	Total number of volume constraints in the ZPR model
tol_{opt}	Tolerance value for optimization process
$V_{\max}^j$	Prescribed maximum volume in the jth volume constraint of the ZPR model
$x_{\max}$	Upper bound for design variables
$x_{\min}$	Lower bound for design variables
$x_i^{(e)}$	Cross-sectional area of member e with material i
$x_{i,L}^{(e),k}$	The lower bound of the eth design variable with material i in the subproblem at optimization step k in the ZPR model
$x_{i,U}^{(e),k}$	The upper bound of the eth design variable with material i in the subproblem at optimization step$k$ in the ZPR model